
Activity of the turbidite levees of the Celtic–Armorican margin (Bay of Biscay) during the last 30,000 years: Imprints of the last European deglaciation and Heinrich events

S. Toucanne^{a,*}, S. Zaragosi^a, J.F. Bourillet^b, F. Naughton^a, M. Cremer^a, F. Eynaud^a and B. Dennielou^b

^aUniversité Bordeaux 1, UMR 5805-EPOC, Avenue des Facultés, F-33405 Talence, France

^bIFREMER, GM/LES, BP70, 29280 Plouzané Cedex, France

*: Corresponding author : S. Toucanne, email address : s.toucanne@epoc.u-bordeaux1.fr

Abstract:

High-resolution sedimentological and micropaleontological studies of several deep-sea cores retrieved from the levees of the Celtic and Armorican turbidite systems (Bay of Biscay — North Atlantic Ocean) allow the detection of the major oscillations of the British–Irish Ice Sheet (BIIS) and ‘Fleuve Manche’ palaeoriver discharges over the last 30,000 years, which were mainly triggered by climate changes.

Between 30 and 20 cal ka, the turbiditic activity on the Celtic–Armorican margin was weak, contrasting with previous stratigraphic models which predicted a substantial increase of sediment supply during low sea-level stands. This low turbidite deposit frequency was most likely the result of a weak activity of the ‘Fleuve Manche’ palaeoriver and/or of a reduced seaward transfer of sediments from the shelf to the margin. However, two episodes of turbiditic activity increase were detected in the Celtic–Armorican margin, during Heinrich events (HE) 3 and 2. This strengthening of the turbiditic activity was triggered by the meltwater releases from European ice sheets and glaciers favouring the seaward transfer of subglacial material, at least via ‘Fleuve Manche’ palaeoriver.

At around 20 cal ka, a significant increase of turbidite deposit frequency occurred as a response to the onset of the last deglaciation. The retreat of the European ice sheets and glaciers induced a substantial increase of the ‘Fleuve Manche’ palaeoriver discharges and seaward transfer of continentally-derived material into the Armorican turbidite system. The intensification of the turbiditic activity on the Celtic system was directly sustained by the widespread transport of subglacial sediments from the British–Irish Ice Sheet (BIIS) to the Celtic Sea via the Irish Sea Basin. A sudden reduction of turbiditic activity in the Armorican system, between ca. 19 and 18.3 cal ka, could have been triggered by the first well known abrupt sea-level rise (‘meltwater pulse’, at around 19 cal ka) favouring the trapping of sediment in the ‘Fleuve Manche’ palaeoriver valleys and the decrease of the seaward transfer of continentally-derived material.

The maximum of turbiditic activity strengthening in the Celtic–Armorican margin, between ca. 18.3 and 17 cal ka, was induced by the decay of European ice sheets and glaciers producing the most extreme episode of the ‘Fleuve Manche’ palaeoriver runoff and a great seaward transfer of subglacial material into the Bay of Biscay. Between ca. 17.5 and 16 cal ka, the turbiditic activity significantly decreased in both Celtic and Armorican turbidite systems in response to a global re-advance of glaciers and ice sheets in Europe. The last episode of ice sheet retreat, between ca. 16 and 14 cal ka, is well expressed in the Celtic system by a new increase of the turbiditic activity. The major episode of sea-

level rise at around 14 cal ka ('Meltwater Pulse 1A'), precluding the seaward transfer of sediments, induced the end of turbiditic activity in both the Celtic and the Armorican system.

Although two main phases of global sea-level rise seem to have had an effect on the Celtic–Armorican margin, this work proposes the BIIS retreat and associated riverine discharges as the main trigger mechanisms of the turbiditic activity in this region during the last 30,000 years.

Keywords: Bay of Biscay; British–Irish Ice Sheet; 'Fleuve Manche'; palaeoriver; last deglaciation; LGM; Heinrich events; turbidites

61 1. INTRODUCTION

62

63 It is widely acknowledged that climate change and resulting sea level oscillations
64 affect in some way the sedimentary processes operating along continental margins and in
65 particular fine grained turbidite systems (Stow et al., 1985). This is the case of non-glaciated
66 margins located at mid- to low latitudes of the eastern North Atlantic (south of 26°N), far way
67 from glaciers (e.g. Weaver et al., 2000). Inversely, the eastern North Atlantic margin (north of
68 56° N) and adjacent submarine fans have been particularly affected by ice-sheet oscillations
69 during the last part of the full-glacial period (e.g. Dowdeswell et al., 2002; Elverhoi et al.,
70 1998). The effectiveness of ice sheets for sustained glaciated margins is recorded in the Bear
71 Island Fan (western Barents Sea – 75°N). The Bear Island Fan has a similar area and volume
72 to the low-latitude fluvially-derived Amazon and Mississippi turbidite systems but a smallest
73 drainage basin (Dowdeswell et al., 2002) suggesting that the adjacent glaciers have a great
74 ability to erode their substrate. Recent surging glaciers (e.g. Gilbert et al., 2002) also show the
75 close connection between sediment supply and ice-sheet oscillations in the high-latitude
76 continental margins.

77 The Celtic and Armorican turbidite systems (Bay of Biscay – 46°N) are located at the
78 transition zone between the eastern North Atlantic glaciated and non-glaciated margins.
79 Weaver and Benetti (2006) have suggested that deep-sea sedimentation in this region is
80 mostly like influenced by sea level changes. However, previous studies on continuous
81 hemipelagic sequences suggest that the Celtic - Armorican margin was affected by the
82 British-Irish Ice Sheet (BIIS) oscillations and in particular during an extreme episode of
83 meltwater discharge via the “Fleuve Manche” palaeoriver at around 18 cal ka (Eynaud et al.,
84 2007; Mojtahid et al., 2005; Zaragosi et al., 2001b). A recent multi-proxy study on three
85 turbidite levees from northern Celtic - Armorican margin also suggests that the BIIS
86 oscillations have had an impact on the deep-sea clastic sedimentation during the last

87 deglaciation and can provide important information about palaeoenvironmental changes at a
88 high resolution time-scale (Zaragosi et al., 2006).

89 However, none of these studies have showed how sedimentary processes operating along
90 this continental margin have been affected by the successive BIIS oscillations occurring
91 between the final stages of the last glacial and the last glacial-interglacial transition (LGIT).
92 The aim of this study is therefore to investigate the relationship between gravity processes in
93 the Celtic and Armorican turbidite systems and the BIIS oscillations for the last 30,000 years.
94 Towards this aim we have performed a high-resolution sedimentological and
95 micropaleontological study from five long piston cores (MD04-2836, MD04-2837, MD03-
96 2690, MD03-2688 and MD03-2695) retrieved in turbidite levees of the Celtic – Armorican
97 margin. In particular, we have estimated the frequency of turbidite deposits which allow
98 quantification of the continental sediment supply removing the problems inherent to local
99 sedimentation rate and/or of coring deformations (Skinner and McCave, 2003).

100 2. GEOLOGICAL AND ENVIRONMENTAL SETTINGS

101

102 The Celtic – Armorican margin is a passive margin composed of two medium-sized deep-
103 sea clastic systems: the Celtic and the Armorican turbidite systems (Droz et al., 1999; Le
104 Suavé, 2000; Zaragosi et al., 2001a; Zaragosi et al., 2000). The Celtic and Armorican turbidite
105 systems are located in the northern and central part of the Bay of Biscay abyssal plain
106 respectively (Figure 1), and have been active since the Early Miocene (Droz et al., 1999;
107 Mansor, 2004). Each system covers about 30,000 km² in water depths ranging from 4100 m to
108 4900 m. The turbidite systems are sustained by more than thirty deep canyons capturing
109 continentally-derived sediments. These canyons converge down to five submarine drainage
110 basins (Bourillet et al., 2003) (Figure 1):

111 - The ‘Grande Sole’ extends from the Goban to the Brenot spurs. The Whittard channel-levee
112 system (Figure 2) is located basinwards of this catchment area;

113 - The ‘Petite Sole’ extends from the Brenot to the Berthois spurs and nourishes the Shamrock
114 channel-levee system (Figure 2);

115 - The ‘La Chapelle’ is located between the Berthois and the Delesse spurs and connects the
116 Blackmud and Guilcher channel-levee systems;

117 - The ‘Ouest Bretagne’ is located between the Delesse and the Bourcart spurs linking
118 downstream with the Crozon channel-levee system;

119 - The ‘Sud Bretagne’, located between the Bourcart and the Folin spurs, is linked downstream
120 to the Audierne channel-levee system (Figure 2).

121 During the last glacial period, the Celtic and Armorican turbidite systems seems to have been
122 particularly influenced by the British-Irish Ice Sheet (BIIS) oscillations and ‘Fleuve Manche’
123 palaeoriver discharges (e.g. Bourillet et al., 2003). It is widely known that the ‘Fleuve
124 Manche’ palaeoriver activity started during the last glacial period, favoured by the lowering

125 of the sea-level stand and by episodes of the BIIS meltwater discharge (Mojtahid et al., 2005;
126 Zaragosi et al., 2001b) which covered Great Britain and Ireland during the last glacial period
127 (e.g. Bowen et al., 2002). The 'Fleuve Manche' palaeoriver had a large catchment area,
128 including the continental palaeodrainage system of major West European palaeorivers such as
129 the Rhine, Meuse, Seine, Somme, Thames and Solent (Bourillet et al., 2003; Lericolais, 1997)
130 (Figure 1).

131 Besides the 'Fleuve Manche' palaeoriver, the Irish Sea Basin seems to have played an
132 important role in sediment supply from the continent to the Celtic - Armorican margin. It is
133 known that the Irish Sea ice stream protruded in the southern Irish Sea and Celtic Sea
134 although its extent is still a matter of debate. Recent simulations (Boulton and Hagdorn, 2006)
135 and geological field studies (Evans and O'Cofaigh, 2003; Hiemstra et al., 2006; O'Cofaigh and
136 Evans, 2007) seem to confirm that the southern limit of this ice stream reached the Isles of
137 Scilly, as previously suggested by Scourse et al. (1991; 1990) (Figure 1).

138 Many studies from marine deep-sea cores have showed that the BIIS was very sensitive to
139 abrupt climatic changes (e.g. Knutz et al., 2007; Peck et al., 2006) and in particular during the
140 last deglaciation (Eynaud et al., 2007; Mojtahid et al., 2005; Zaragosi et al., 2006; Zaragosi et
141 al., 2001b). This hypothesis has been confirmed by several continental studies which reveal a
142 progressive but complex decay of the BIIS during the last deglaciation (McCabe and Clark,
143 1998; McCabe et al., 2007b).

144 3. MATERIALS AND METHODS

145
146 Five long piston cores (Table 1) were retrieved by using the ‘Calypso’ corer in the Celtic
147 – Armorican margin during the MD133-SEDICAR (Bourillet and Turon, 2003) and the
148 MD141-ALIENOR (Turon and Bourillet, 2004) oceanographic cruises on board the R/V
149 Marion Dufresne (IPEV). Cores MD03-2688, MD03-2690 and MD03-2695 were recovered in
150 the Crozon, Guilcher and Audierne turbidite levees (Armorican turbidite system) while cores
151 MD04-2836 and MD04-2837 were collected in the Whittard and Shamrock turbiditic levees
152 (Celtic turbidite system) (Figure 1 and 2). Previous studies on this region have shown that
153 some of these turbidite levees are mainly composed of a complex sedimentological succession
154 of turbiditic sequences alternating with ice-rafted laminae and hemipelagic layers (Zaragosi et
155 al., 2006).

156 3.1. Chronostratigraphy

157
158 The age models for cores MD03-2688, MD03-2690, MD03-2695 and MD04-2836 have
159 been determined based on foraminiferal stratigraphy, AMS dating and by using additional
160 control points from the reference core MD95-2002 (Table 2). The age model of core MD95-
161 2002 was based on 20 ¹⁴C AMS ages spanning the last 30 ka (Table 2) (Auffret et al., 2002;
162 Grousset et al., 2000; Zaragosi et al., 2006; Zaragosi et al., 2001b).

163 Cores were sub-sampled with a sample spacing of 5 to 20 cm for micropaleontological
164 analysis along the hemipalegic layers. These hemipelagic layers are not contaminated by
165 reworked material and represent intervals of continuous sedimentation. The subsamples were
166 then dried, weighed and washed through a 150 µm mesh sieve. At least 300 polar foraminifera
167 *Neogloboquadrina pachyderma* (s) were counted jointly with a number of other planktonic
168 species in order to determine the relative abundances (%) of this polar species. Previous
169 studies on this region have shown the suitable use of *N. pachyderma* (s) to reconstruct drastic

170 sea-surface changes which are stratigraphically contemporaneous with major climatic events
171 (Mojtahid et al., 2005; Peck et al., 2007; Zaragosi et al., 2001b).

172 Thirty four accelerator mass spectrometer (AMS) ^{14}C dates were obtained from cores
173 MD03-2688, MD03-2690, MD03-2695 and MD04-2836 (Table 2).

174

175 **3.2. Sedimentological analyses**

176
177 The sedimentological analyses of the Celtic – Armorican deep-sea cores consists firstly of
178 visual description and X-ray analysis obtained with a SCOPIX image processing tool (Migeon
179 et al., 1999). Additionally, grain-size analysis were performed using a MalvernTM Supersizer
180 ‘S’. Finally, microscopical observations of about ten thin-sections (10 cm long) of
181 impregnated sediments selected from well-preserved and representative sedimentary facies
182 were performed using a fully automated LeicaTM DM6000B Digital Microscope. The last
183 method has been recently detailed in Zaragosi et al. (2006).

184 In order to understand the activity of the Celtic and Armorican turbidite systems, we have
185 detected and quantified the number of turbiditic deposits in the Whittard, Guilcher, Crozon
186 and Audierne turbidite levees. For this, we firstly observed several thin sections of
187 impregnated sediments representing distinctive alternated facies of ice-rafted, turbiditic
188 deposits and hemipelagic layers (Figure 3). Secondly, we have determined the criteria to
189 distinguish each facies *via* microscope and X-ray imagery. Finally, we applied these criteria to
190 distinguish each facies in all cores using X-ray imagery. Indeed, microscopic observation of
191 IRD laminae reveals heterogeneous and scattered angular lithic grains within fine-bioturbated
192 clay while fine (mm-thick) and slightly dark layers are observed in the X-ray imagery (Figure
193 3). Turbiditic deposits are generally thicker (mm-thick to cm-thick) than IRD laminae and
194 present usually sharply eroded basal contacts. The progressive transition from very dense

195 (dark) contacts to a slightly lighter (grey) top of sequences, visible on X-ray imagery, is
196 associated with the typical fining-up trend of turbiditic deposits (Bouma, 1962; Stow and
197 Piper, 1984) (Figure 3).

198 Each turbiditic deposit of cores MD04-2836, MD03-2690, MD03-2688 and MD03-2695
199 has been counted using X-ray imagery. Turbidites have not been counted in core MD04-2837
200 because this record presents important disturbances linked to coring stretching. Following
201 this, we have quantified the turbidite deposit frequency on the Whittard, Guilcher, Crozon and
202 Audierne levees per 1000 years. We assumed that this quantification represents the minimum
203 value of turbidite frequency because of possible erosive losses and/or non-deposit events (i.e.
204 by-pass).

205 4. RESULTS

206 4.1. Chronological framework

207
208 It is usually difficult to reconstruct an accurate stratigraphy in turbidite levees because
209 these environments are mainly composed of reworked sedimentary material. Therefore, we
210 have used the abundance peaks of *N. pachyderma* (s) determined in well preserved
211 hemipelagic material as primary tool to establish the age model of cores MD04-2836, MD04-
212 2837, MD03-2688, MD03-2690 and MD03-2695. This method allows the detection of several
213 paleoclimatic events during the end of the Marine Isotopic Stages (MIS) 3, MIS 2 and MIS 1:
214 Heinrich events (HE 3, HE 2 and HE 1), Last Glacial Maximum (LGM), Greenland
215 Interstadial 1 (GIS1) / Bölling-Alleröd (B-A), Younger Dryas (YD) and the Holocene (Figure
216 4).

217 The maximum expansion of the polar foraminifera *N. pachyderma* (s) in the Celtic–
218 Armorican margin between ca. 18.3 and 16 cal ka (Figure 4), suggesting extremely cold sea
219 surface waters, is contemporaneous with the presence of ice rafted detritus (IRD) in the
220 reference core MD95-2002 (Zaragosi et al., 2001b). Although IRD are detected between ca.
221 18.3 and 16 cal ka, their maximum expression occurred within the interval 17-16 cal ka. The
222 age limits of this cold episode are synchronous with those proposed by Elliot et al. (2001) for
223 Heinrich (HE) 1 event elsewhere in the North Atlantic region. The other episodes of *N.*
224 *pachyderma* (s) maximum expansion (~90-100%) occurring at ca. 23.5-26 cal ka and at ca.
225 30-32 cal ka are also synchronous with the age limits of HE 2 and HE 3, respectively (Elliot et
226 al., 2001). We assume therefore that these cooling events detected in the Celtic-Armorican
227 margin are most likely the result of the impact of Heinrich events. Previous works on the
228 eastern North Atlantic (e.g. Bond et al., 1992; Eynaud et al., 2007) have shown a sea surface
229 cooling episode preceding the maximal arrival of IRD. Other records from the mid-latitudes

230 of the North Atlantic region have shown the same complex pattern in both marine and
231 terrestrial environments, which have been associated to the well known Heinrich events (e.g.
232 Bard et al., 2000; Chapman et al., 2000; Naughton et al., 2007; Naughton et al., submitted).

233 The Younger Dryas cold period is also defined by the increase of the *N. pachyderma* (s).
234 However, an intriguing sedimentary hiatus is observed at around this period in cores MD03-
235 2688 and MD03-2695 (Figure 4). The planktonic foraminiferal assemblages show that the
236 Early Holocene and Bølling-Allerød periods are well recorded in both cores (Duprat, *comm.*
237 *pers.*).

238 Furthermore, radiocarbon results have confirmed that core-to-core correlations, based on
239 abrupt increases in abundances of *N. pachyderma* (s), represent the temporal limits of the cold
240 episodes that punctuated the final part of the last glacial period (Table 2 and Figure 4).

241 The age model of core MD03-2688 indicates that this core covers the last ca. 34 cal ka
242 (~29.1 ¹⁴C ka); core MD03-2695 extends back to ca. 33.5 cal ka (~28.7 ¹⁴C ka) and core
243 MD03-2690 to ca. 26 cal ka (~22 ¹⁴C ka); and core MD04-2836 spans ca. 20.4 cal ka (~17.3
244 ¹⁴C ka) (Figure 4 and Table 2).

245

246 **4.2. Evolution of sedimentary conditions**

247

248 The detailed sedimentological analysis (visual description, X-ray imagery, grain-size
249 measurements and thin section analysis) of the studied cores has allowed the identification of
250 six lithofacies (Figure 5, 7 and 8). These lithofacies represent the evolution of the sedimentary
251 conditions on the Whittard, Blackmud, Guilcher, Crozon and Audierne levees during the last
252 30,000 years (Figure 5):

253 *Lithofacies 1*, between 0 and 8 cal ka (Mid- and Late-Holocene), is constituted by
254 homogeneous, structureless marly ooze containing a temperate foraminiferal assemblage

255 (*Globigerinoides ruber*, *Globigerina bulloides*, *Globorotalia hirsuta*, *Globorotalia*
256 *truncatulinoides*, *Orbulina universa*) (Figure 5). This lithofacies forming the modern deep-sea
257 Bay of Biscay seafloor has been interpreted on the turbidite levees as a pelagic to hemipelagic
258 drape deposits without significant turbidite supplies from the continental shelf (Zaragosi et al.,
259 2006).

260 *Lithofacies 2*, between ca. 8 and 15.5 cal ka, consists of homogeneous structureless
261 clay interbedded with some centimetre-scale silt to very fine sand layers (Figure 5).
262 Sedimentation rates range from 270 to 370 cm.ka⁻¹ and reach 770 cm.ka⁻¹ in core MD04-2836
263 (Figure 6). Beds display a sharply erosive basal contact and are normally graded, with a basal
264 grain-size median ranging from 20 to 80 µm in core MD04-2836, 40 to 80 µm in core MD03-
265 2690 and 60 to 140 µm in core MD03-2688. According to Stow and Piper (1984), these beds
266 represent silt-mud turbidites deposited from the overflow of turbidity currents while
267 homogeneous clay are interpreted as hemipelagic deposits.

268 *Lithofacies 3*, between ca. 15.5 and 17 cal ka, ca. 23.5 and 26 cal ka and ca. 30.5 and 32
269 cal ka., shows a monospecificism of the polar foraminifera *N. pachyderma* (s) and contains
270 frequent thinning- and fining-upward sequences of very fine sand and silt deposits with
271 erosive basal contacts (Figure 5). These sequences are interpreted as fine-grained turbidites.
272 Turbidite layers are thin (1 to 10 cm) and their basal grain-size ranges from 40 to 160 µm in
273 core MD04-2836, 50 to 140 µm in core MD03-2690, 30 to 110 µm in core MD03-2688 and 15
274 to 100 µm in core MD032695. Numerous IRD-rich millimetre-scale clay layers are also
275 interbedded with the turbidite sequences. Sedimentation rates range from 110 to 500 cm.ka⁻¹
276 in cores MD04-2836 and MD03-2690 respectively (Figure 6). Lithozone 3 reveals periods of
277 important turbidite deposits associated with numerous ice-rafting events on the sedimentary
278 levees of the Celtic – Armorican margin.

279 *Lithofacies 4*, between ca. 17 and 18.3 cal ka, is an ultra-laminated sediment composed of
280 IRD-rich millimetre-scale clay layers and fine fining-upward silty laminae with sharp basal
281 contacts (Figure 5 and 7). Some silty to very fine sandy deposits are also observed and show
282 thin cross-rippled laminations. These laminations are interpreted to be of turbiditic origin.
283 Their basal grain-size ranges from 40 to 140 μm in cores MD04-2836 and MD03-2690, 20 to
284 120 μm in core MD03-2688 and 20 to 180 μm in core MD03-2695. Load casts and flame
285 structures are commonly present at the lower contacts of the turbidites. A monospecificism of
286 *N. pachyderma* (s) is also described in lithofacies 4. Sedimentation rates are extremely high
287 ($>600 \text{ cm.ka}^{-1}$) and reach up to 950 cm.ka^{-1} in core MD03-2695 (Figure 6). Lithofacies 4
288 reveals a high sediment supply period produced by very frequent turbidity currents in the
289 channel-levee systems and numerous ice-rafting events.

290 *Lithofacies 5*, between ca. 18.3 cal ka and ca. 20 cal ka, is characterized by homogeneous
291 structureless clay interbedded with some fining-upward millimetre- to centimetre-scale silt to
292 sand deposits with erosive basal contacts (Figure 5). These sequences are interpreted as fine-
293 grained turbidites. Some parts of the top of lithozone 5 are laminated and represent a
294 transition zone between the ultra-laminated lithofacies 4 and the base of the lithofacies 5
295 which is mostly composed of scattered centimetre-scale turbidites. The grain-size of the base
296 of turbidite beds ranges from 40 to 160 μm in core MD04-2836, 50 to 190 μm in core MD03-
297 2690, 60 to 240 μm in core MD03-2688 and 50 to 230 μm in core MD03-2695. Mean
298 sedimentation rates range from 290 to 375 cm.ka^{-1} except in core MD04-2836 where it
299 reaches 545 cm.ka^{-1} (Figure 6). Lithofacies 5 shows hemipelagic sedimentation interbedded
300 with some turbidites deposits that are more massive and more spaced in its basal part, thus
301 defining a transition sedimentary facies between lithofacies 4 and lithofacies 6.

302 *Lithofacies 6* was deposited between ca. 20 and 34 cal ka, except during ca. 23.5 – 26 cal
303 ka and ca. 30.5 – 32 cal ka periods which corresponds to lithofacies 3. Lithozone 6 is

304 dominated by massive, fining-upward silt to sand deposits, interpreted as turbidites (Figure 5
305 and 8). Grain-size appears to be similar to that characterising lithofacies 5. However,
306 turbidites of lithofacies 6 are thicker (centimetre to decimetre-scale) than turbidites of
307 lithofacies 5. Sedimentation rates are moderate to low with values ranging from 15 to 100
308 cm.k^{-1} (Figure 6). Lithofacies 6 reveals a period of rare but massive turbidity current activity.
309

310 **4.3. Turbidite deposit frequency**

311
312 The frequency of the turbiditic deposits (turb.k^{-1}) has been estimated from cores MD04-
313 2836, MD03-2690, MD03-2688 and MD03-2695 for the last 30 ka (Figure 6, 9 10 and 11).

314 Three main periods of turbiditic activity are observed:

315 a) From ca. 33 to 20 cal ka, there is a general low turbiditic activity in the Guilcher,
316 Crozon and Audierne channel levee systems. The turbidite deposit frequency ranges from 0 to
317 40 turbidites per thousand years (turb.k^{-1}). A moderate frequency of turbiditic deposits
318 occurred during HE 3 and HE 2 (30 to 40 turb.k^{-1}) while low turbiditic activity (max. 15
319 turb.k^{-1}) is associated with the end of MIS 3 and the early- and mid-LGM (Figure 6 and 9).

320 b) Between ca. 20 to 17 cal ka, there is a general huge increase in the frequency of the
321 turbidite deposits (75 turb.k^{-1} in core MD03-2688 and 230 turb.k^{-1} in core MD04-2836)
322 (Figure 6, 9 and 10). A higher resolution study of the frequency of the turbidite deposits
323 (number of turbidites per 250 years), in core MD03-2688, shows a sudden episode of turbidite
324 deposit frequency decrease between ca. 19 and 18.3 cal ka (Figure 10). The turbiditic activity
325 reached a maximum intensity between ca. 18.3 to 17 cal ka in all cores independently of the
326 time resolution used to calculate those frequencies (Figure 6, 9 and 10).

327 c) From ca. 17 to 16 cal ka, there is a sharp decrease of the turbiditic activity in all cores.
328 The turbidite deposit frequency reached 60 to 120 turb.k^{-1} on the Guilcher, Crozon and

329 Audierne levees and only 25 turb.ka⁻¹ on the Whittard levee between 17 and 16 cal ka (Figure
330 6, 9, 10 and 11).

331 d) From ca. 16 to 0 cal ka, although there is a gradual decrease of the turbiditic activity in
332 most areas (Figure 6, 9, 10 and 11), Whittard records shows a significant re-activation of
333 gravity processes at the beginning of this interval. Indeed, turbidite deposit frequency of core
334 MD04-2836 reaches 130 turb.ka⁻¹ between ca. 16 and 14 cal ka while attaining only 25
335 turb.ka⁻¹ between ca. 17 – 16 cal ka and 8 turb.ka⁻¹ between ca. 14 – 13 cal ka (Figure 11).

336

337

338

339

340 **5. DISCUSSION**

341 **Implications of the BIIS and ‘Fleuve Manche’ palaeoriver activities in the Celtic –**
342 **Armorican margin during the last 30 ka**

343

344 The high-resolution sedimentological and micropaleontological study of several marine
345 deep-sea cores retrieved on the turbidite levees of the Whittard, Blackmud, Guilcher, Crozon
346 and Audierne channel-levee systems allows the detection of the major BIIS oscillations and
347 ‘Fleuve Manche’ palaeoriver discharges during the last 30 ka. The turbidite deposit frequency
348 estimated in MD04-2836, MD03-2690, MD03-2688 and MD03-2695 deep-sea cores reflects
349 important oscillations of sediments supply into the Celtic and Armorican turbidite systems
350 between 30 ka and 14 ka BP (Figure 6 and 9).

351 The last glacial period is marked by the long-term increase of the global ice volume,
352 contemporaneous with the global sea-level fall (Chappell, 2002; Lambeck et al., 2002). The
353 last sea-level lowstand, contemporaneous with the final stages of the global ice expansion
354 occurred between ca. 30 and ca. 20 cal. ka (Lambeck et al., 2002). However, during this
355 interval, several millennial-scale climate oscillations have been observed in both Greenland
356 and North Atlantic records (Bond et al., 1993; Dansgaard et al., 1993) producing substantial
357 sea-level changes (Siddall et al., 2003). In this work, we define the LGM as a period of
358 relatively stable climate that occurred between HE 2 and HE 1 following the EPILOG (Mix et
359 al., 2001) and MARGO (Kucera et al., 2005) suggestions.

360 It is commonly accepted that sea-level lowstand conditions favoured the seaward sediment
361 transfer from the continent to the deep-sea turbidite systems (e.g. Posamentier and Vail,
362 1988). Therefore, we should expect to detect a maximum of the turbidite frequency in the
363 Celtic and Armorican turbidite systems synchronous with the last lowest sea-level stand. Our
364 data shows, on the contrary, that there is a general weak sediment supply to the Celtic and

365 Armorican turbidite systems between ca. 30 and ca. 20 cal. ka (Figure 6 and 9). The low
366 turbidite deposit frequency within ca. 30 and 20 cal. ka in the Celtic - Armorican margin can
367 probably be due to weak runoff rates of the 'Fleuve Manche' palaeoriver and/or to low
368 seaward sediment transfer which was probably blocked on the shelf as a response to the
369 deposition of sand banks in the Celtic sea (Reynaud et al., 1999). Nonetheless, the presence of
370 some turbidite sequences in this region is most likely the result of sediment seaward transfer
371 from the delta located in the 'Fleuve Manche' palaeoriver mouth (Lericolais, 1997; Zaragosi
372 et al., 2001a). Two episodes of turbidite frequency increase contemporaneous with HE 3 and
373 HE 2 punctuated the general low turbidite activity period (Figure 6, 9 and 10). This increase
374 of turbiditic activity during HE 3 and HE 2 was likely the result of an increase of seaward
375 transfer of subglacial sediment as a response to meltwater releases from surrounded ice sheets
376 and glaciers, confirming what has been previously proposed by climate simulations (e.g.
377 Clarke et al., 1999; Forsström and Greve, 2004) as well as by sedimentological studies on the
378 eastern Canadian margin (e.g. Hesse et al., 2004; Rashid et al., 2003).

379 A significant increase of sediment supply shown by the increase of the turbidite deposit
380 frequency is observed since ca. 20 cal ka in cores MD04-2836 (i.e. in the Celtic turbidite
381 system), MD03-2690, MD03-2688 and MD03-2695 (i.e. in the Armorican turbidite system)
382 (Figure 6 and 9). The quantity of sediment supply into the Celtic turbidite system is higher
383 than that of the Armorican turbidite system.

384 The 'Grande Sole' drainage basin was connected to the Celtic Sea (Figure 1) funnelling
385 substantial volume of sediment directly released by the BIIS and the Irish Sea ice stream
386 (Bowen et al., 1986; Eyles and McCabe, 1989) into the Celtic turbidite system via the Irish
387 Sea Basin. The 'Cooley Point Interstadial', starting at ca. 20 cal ka (~ 16.7 ^{14}C ka BP,
388 (McCabe and Clark, 1998)), characterises the beginning of the BIIS deglaciation and induced
389 the widespread transport of subglacial sediments to the south-east Irish ice-margin as

390 previously suggested by several continental records (Bowen et al., 2002; McCabe et al.,
391 2005). The high turbiditic activity in the Whittard channel synchronous with the major
392 episode of the Irish Sea ice stream retreat (Figure 11) suggests that the Irish Sea Basin was
393 probably affected by fully marine conditions, favouring the direct seaward transfer of
394 sediments from the BIIS. These fully marine conditions were attained because the isostatic
395 depression of the Irish Sea Basin vastly exceeded the eustatic lowering as suggested by Clark
396 et al. (2004) and McCabe et al. (2007a; 2007b).

397 Although the turbidite deposit frequency in the Armorican turbidite system is lower
398 than that recorded in the Celtic system, an increase of the turbiditic activity has been also
399 detected in cores MD03-2690, MD03-2688 and MD03-2695 at around 20 cal ka (Figure 6, 9
400 and 10). This increase of the turbidite deposit frequency in the Armorican turbidite system
401 suggests the strengthening of the 'Fleuve Manche' palaeoriver discharges at around 20 cal ka.
402 Seismic records from this region show the presence of Neogene fluvial palaeovalleys in the
403 present-day shelf (Figure 1), between the 'Fleuve Manche' palaeoriver and canyons of the
404 Armorican margin (Bourillet et al., 2003). This suggests that these sub-environments were
405 directly connected in the past, favouring the great seaward transfer of sediments from the
406 'Fleuve Manche' palaeoriver via the numerous canyons which composed the 'La Chapelle',
407 'Ouest Bretagne' and 'Sud Bretagne' drainage basins (Figure 1 and 2). Furthermore, previous
408 studies on this region detected an increase of *Pediastrum sp.* concentration (freshwater alga)
409 (Zaragosi et al., 2001b) and of BIT-index (Branched and Isoprenoid Tetraether) (Ménot et al.,
410 2006) reflecting the introduction of high quantities of fluvial terrestrial organic material in the
411 Armorican margin contemporaneous with the increase of turbiditic activity in this area
412 (Figure 10). Additionally, recent simulations have shown that tides and tidal currents of the
413 Celtic - Armorican shelf also contributed to the seaward transfer of continental material
414 between 20 and 10 ka (Uehara et al., 2006).

415 The strengthening of the 'Fleuve Manche' palaeoriver discharges was probably induced
416 by the retreat of the BIIS, the European glaciers and the south-western part of the
417 Fennoscandian ice sheet. The well known episodes of glacier decay in Scandinavia
418 (Rinterknecht et al., 2006), Poland (Marks, 2002) and in the European Alps (Hinderer, 2001;
419 Ivy-Ochs et al., 2004) at around ca. 20 cal ka corroborate our hypothesis.

420 The retreat and melting of the European ice sheets and glaciers at ca. 20 cal ka contributed
421 to an abrupt sea-level rise, known as a 'meltwater pulse' at around 19 cal ka (19-ka MWP)
422 (Clark et al., 2004; Yokoyama et al., 2000). This abrupt episode lasted 500 years and sea level
423 rise amounted to over 15 m (Yokoyama et al., 2000) favouring the trapping of sediments in
424 the 'Fleuve Manche' palaeoriver valleys. Synchronously, the decrease of both BIT-index and
425 *Pediastrum sp.* concentration in the neighbouring core (MD95-2002) (Ménot et al., 2006;
426 Zaragosi et al., 2001b) (Figure 10) suggests a decrease of continentally-derived material to the
427 Armorican margin, also supporting the idea of reduced 'Fleuve Manche' discharges in the
428 northern part of the Bay of Biscay.

429 Following this, the observed abrupt increase of sediment supply in the Celtic and
430 Armorican turbidite systems at ca. 18.3 cal ka (Figure 6, 9, 10 and 11) was most likely the
431 result of a seaward sediment transfer increase from the south-east Irish ice-margin and an
432 intensification of the 'Fleuve Manche' palaeoriver runoff, respectively. In the Armorican
433 turbidite system, the highest turbidite deposit frequency is synchronous with the maximal
434 arrival of continental material as demonstrated by BIT-index (Ménot et al., 2006) and
435 *Pediastrum sp.* concentration (Zaragosi et al., 2001b) (Figure 10). This suggests that the
436 'Fleuve Manche' discharges increased drastically at around 18.3 cal ka confirming what has
437 been previously proposed by Zaragosi et al. (2001b) and Ménot et al. (2006). This episode of
438 high riverine discharges, occurring at ca. 18.3 cal ka, was clearly more intense than that
439 characterizing the beginning of the deglaciation (ca. 20 cal ka) (Figure 6, 9 and 10) and was

440 also likely the result of the European glacier retreat. Several studies have shown that
441 important environmental changes leading to a substantial retreat of the BIIS occurred in the
442 north and north-western UK margin (Knutz et al., 2002a; Knutz et al., 2002b; Wilson et al.,
443 2002), contemporaneous with the maximum decay of the Fennoscandian ice sheet at ca. 18.3
444 cal ka (Dahlgren and Vorren, 2003; Lekens et al., 2005; Nygard et al., 2004). The deposition
445 of one ultra-laminated facies in the Celtic – Armorican margin between ca. 18.3 cal ka and 17
446 cal ka (lithofacies 4 – Figure 5) reveals that a significant environmental change has had an
447 impact in northern and southern part of the glacially-influenced European margin. This facies
448 has been recognized as marine ‘varves’ resulting from episodic cycles between meltwater
449 discharges and iceberg calving (Zaragosi et al., 2006).

450 Between ca. 17.5 and 16 cal ka, there was a decrease of the turbiditic activity in the Celtic
451 turbidite system (Figure 6, 9 and 11) which was contemporaneous with the two main general
452 re-advance phases of the BIIS: the ‘Clogher Head’ and ‘Killard Point’ stadials (after 15 and
453 until ~ 13 ^{14}C ka BP), detected in the northern Irish Sea Basin by McCabe et al. (2007b). This
454 suggests that sub-glacial material transfer from the BIIS to the ‘Grande Sole’ drainage basin
455 was most likely reduced during re-advance episodes of the BIIS. These episodes were
456 synchronous with the re-advance of the Fennoscandian ice-sheet and central European
457 glaciers (Alps, Jura) (Buoncristiani and Campy, 2004; Everest et al., 2006; Ivy-Ochs et al.,
458 2006; Knies et al., 2007). The rapid decrease of the turbidite deposit frequency in the
459 Armorican turbidite system (Figure 6, 9 and 10) reveals a substantial decrease of the ‘Fleuve
460 Manche’ palaeoriver runoff, in response to the episodic ‘pause’ of the last deglaciation.

461 The resumption of the last deglaciation is particularly well expressed in the Celtic
462 turbidite system record during the well known Bölling-Alleröd episode. Indeed, the last major
463 decay of the BIIS, associated with the ‘Stagnation Zone Retreat’ and the ‘Rough Island
464 Interstadial’ episodes detected in the northern Irish Sea Basin (McCabe et al., 2005; McCabe

465 et al., 2007b), induced a relatively huge increase of the turbiditic activity in the Celtic
466 turbidite system, between ca. 16 and 14 cal ka (Figure 11). Besides the last stages of the BIIS
467 decay, the Celtic - Armorican margin was also affected by a rapid and sustained rise of the
468 global sea-level from 16 to 12.5 cal ka (Lambeck et al., 2002). Indeed, the cessation of
469 turbiditic activity on the Celtic - Armorican margin occurred during or after the episode of
470 maximum sea-level rise (Figure 10), known as the 'Meltwater Pulse 1A' (MWP 1A - ca. 14
471 cal ka) (Fairbanks, 1989) contributing to the disappearance of the 'Fleuve Manche'
472 palaeoriver. Moreover, the increase of dry conditions in Europe during the Younger Dryas at
473 around 13 cal ka (e.g. Watts, 1980) also decreased the seaward transfer of fluvially-derived
474 sediment onto the Celtic - Armorican margin.

475 The comparison of the turbiditic activity between the Celtic turbidite system and the
476 Laurentian Fan, which extends at the outlet of the Laurentide Ice Sheet (LIS) (Skene and
477 Piper, 2003), reveals a similar sedimentary pattern over the last deglaciation. Two main
478 phases of turbidite deposition occurred at the end of the LGM and after ca.16 cal ka,
479 bracketing a huge reduction of sediment supply at around 16.5 cal ka. Despite a short time lag
480 between the BIIS and the LIS oscillations over the last deglaciation (McCabe and Clark,
481 1998), the similarity of both turbiditic records from the Laurentian Fan and the Celtic system
482 suggests that seaward transfer of glacially-derived material to the deep-sea North Atlantic
483 have been clearly forced by the combined effect of global climate changes and amphi-North
484 Atlantic ice sheets oscillations for at least the last 20,000 years.

485 **6. CONCLUSIONS**

486

487 The high-resolution sedimentological (including turbidite frequency analysis) and
488 micropaleontological studies performed in the Celtic - Armorican margin document the
489 evolution of the turbidite systems in this region over the last 30,000 years. Changes in the
490 frequency of turbidite deposits in the Celtic - Armorican margin were mainly triggered by the
491 British – Irish Ice Sheet (BIIS) and European glaciers oscillations (advance and retreat
492 episodes). The retreat of the BIIS and European glaciers favoured the transfer of
493 continentally-derived material *via* the Irish Sea ice stream and the ‘Fleuve Manche’
494 palaeoriver into the Celtic and the Armorican systems respectively. Inversely, the BIIS and
495 European glaciers advances preclude the introduction of large amounts of meltwater into the
496 ‘Fleuve Manche’ palaeoriver, reducing drastically the seaward transfer of sediments in the
497 Bay of Biscay. This evidence, contrasting with stratigraphic models which predict that
498 turbidite systems are mainly controlled by sea level changes, confirms that glacially-
499 influenced turbidite systems are largely controlled by ice sheets and glaciers oscillations.
500 However, the synchronicity between turbidite deposit frequency reduction and the abrupt
501 meltwater pulse episode (19-ka MWP) suggests that this drastic sea-level rise would have
502 favoured the trapping of sediments in the ‘Fleuve Manche’ palaeoriver. Similarly, after the
503 last stage of the BIIS decay a second sudden episode of sea-level rise (MWP 1A) contributed
504 to the end of the ‘Fleuve Manche’ palaeoriver discharges and consequent turbiditic activity in
505 the Celtic - Armorican margin.

506 **ACKNOWLEDGEMENTS**

507

508 The authors warmly thank G. Chabaud, G. Floch, R. Kerbrat, B. Martin, M. Rovere, J. Saint
509 Paul and O. Ther for their technical support and J. Duprat and A. Van Toer for their useful
510 assistance to the biostratigraphic approach. We thank also G. Ménot for data of the BIT-
511 index; P. De Deckker, M. Gaudin and M.F. Sánchez Goñi for valuable comments and
512 language improvement; and the crew and scientific teams of MD133/SEDICAR and
513 MD141/ALIENOR cruises on the 'R/V Marion Dufresne' (IPEV) for the recovery of the
514 long-piston cores. We acknowledge financial support by the French Programme 'GDR
515 MARGES' and 'RELIEFS DE LA TERRE', the 'ARTEMIS' ¹⁴C AMS French Project and
516 the ANR 'IDEGLACE'. We finally acknowledge A.M. McCabe, J.D. Scourse and Editor
517 D.J.W. Piper for their helpful comments which greatly improved this paper. This is an UMR
518 5805 'EPOC' (Bordeaux 1 University - CNRS) contribution n°1637.

519 **FIGURE CAPTION**

520

521 Figure 1: Physiography of the Celtic - Armorican margin (north-western Europe) during the
522 Last Glacial Maximum (LGM). (1) extent of the British – Irish Ice Sheet (BIIS) (Bowen et al.,
523 2002); (2) southern extent of the Irish Sea ice stream proposed by Scourse and Furze (2001);
524 (3) extent of the European Alps glacier; (4) ‘Fleuve Manche’ palaeoriver (Bourillet et al.,
525 2003); (5) Celtic sand banks (Reynaud et al., 1999); fluvial palaeovalleys (blue dashed lines)
526 (Larsonneur et al., 1982); submarine drainage basins: (A) ‘Grande Sole’, (B) ‘Petite Sole’, (C)
527 ‘la Chapelle’, (D) ‘Ouest Bretagne’, (E) ‘Sud Bretagne’ (Bourillet et al., 2003); (6) Celtic
528 turbidite system (Droz et al., 1999; Zaragosi et al., 2000); (7) Armorican turbidite system
529 (Zaragosi et al., 2001a). Red circles indicate the core locations.

530

531 Figure 2: Shaded morphologic map of the Celtic – Armorican margin. White circles and
532 associated numbers indicate core locations.

533

534 Figure 3: Recognition of turbiditic and ice-rafted laminae on X-ray imagery and on the
535 microscope using thin-sections of impregnated sediment.

536

537 Figure 4: Abundance (%) of foraminifera *N. pachyderma* (s.) in cores MD04-2836, MD04-
538 2837, MD03-2690 (Zaragosi et al., 2006), MD03-2688, MD03-2695 (this study) and MD95-
539 2002 (Zaragosi et al., 2001b). Black triangles indicate the depth of samples used for AMS
540 dating. Blue shading corresponds to cold periods. Dashed red lines represent core-to-core
541 correlation using the limits of cold episodes. Hol: Holocene, YD: Younger Dryas, BA:
542 Bölling-Alleröd, HE: Heinrich events (1 to 3), LGM: Last Glacial Maximum.

543

544 Figure 5: Examples of some representative X-rayed slabs of lithofacies 1 to 6.

545

546 Figure 6: Evolution of sedimentation rates (continuous black line - cm.ka^{-1}) and of turbidite
547 deposit frequency (continuous red line – turb.ka^{-1}) in cores MD04-2836, MD03-2690, MD03-
548 2688 and MD03-2695. Although sedimentation rates must be considered with precaution
549 because of frequent oversampling in Calypso piston cores (Skinner and McCave, 2003), the
550 resulting curves parallel those of the turbidite deposit frequency suggesting that sedimentation
551 rates can be considered as fairly valid.

552

553 Figure 7: Example of a thin-section of impregnated sediment (left) from lithofacies 4 in core
554 MD03-2690, X-ray (middle) and grain-size measurements (right). D50 (continuous line) =
555 grain-size at which 50% of sample is finer; D90 (dashed line) = grain-size at which 90% of
556 sample is finer. Open circles represent the chosen samples used for grain-size analysis. Black
557 layers represent turbidite deposits in the X-ray imagery.

558

559 Figure 8: Example of an X-rayed slab (left) from lithofacies 6 in core MD03-2695 and grain-
560 size measurements (right). D50 (continuous line) = grain-size at which 50% of sample is
561 finer; D90 (dashed line) = grain-size at which 90% of sample is finer. Open circles represent
562 the chosen samples used for grain-size analysis. Black layers represent turbidite deposits in
563 the X-ray imagery.

564

565 Figure 9: Evolution of the turbidite deposit frequency (histograms – turb. ka^{-1}) using time
566 slices (1 ka) of the age models of cores MD04-2836, MD03-2690, MD03-2688 and MD03-
567 2695. The continuous red line represents the frequency of turbidite deposits (turb. ka^{-1})
568 calculated by using two consecutive control-points.

569

570 Figure 10: Comparison between: (A) sedimentologic data of core MD03-2690 and (B, C)
571 palaeoclimatic records of core MD95-2002 between 27 and 12 cal. ka. (A) Histogram
572 represents the turbidite deposit frequency with a 250-year resolution (turb./0.25 ka). Red
573 curves show the relative sea-level evolution (m.) described by Fairbanks et al. (1989)
574 (continuous line) and by Waelbroeck et al. (2002) (dashed line). Blue line represents the rate
575 of sea-level rise (mm.a^{-1}) and the 'Meltwater Pulse 1A' (MWP 1A - ca. 14 cal ka) (Fairbanks,
576 1989). (B) BIT-index (Ménot et al., 2006) and *Pediastrum* sp. abundances ($\#\text{.cm}^{-3}$) (Eynaud,
577 1999; Zaragosi et al., 2001b). (C) Abundances of IRD $> 150 \mu\text{m}$ ($\#\text{/g.}$) and *N. pachyderma*
578 (s.) (%) (Zaragosi et al., 2001b).

579

580 Figure 11: Comparison between turbidite deposit frequency in the Celtic turbidite system
581 (core MD04-2836) (this study) and the BIIS oscillations in the Irish Sea Basin (McCabe et al.,
582 2007b). Continuous red line show the frequency of turbidite deposits (turb.k^{-1}) between two
583 consecutive control-points of the age-model of core MD04-2836 while the histogram show
584 the turbidite deposit frequency using a time slicing of 1 ka. 1: 'Cooley Point Interstadial'
585 (from ≥ 16.7 to ≤ 15 ^{14}C ka BP); 2: 'Clogher Head Stadial' (from ≥ 15 to ≤ 14.2 ^{14}C ka BP); 3:
586 'Linns Interstadial' (~ 14.2 ^{14}C ka BP); 4: 'Killard Point Stadial' (from ≥ 14.2 to ~ 13.0 ^{14}C ka
587 BP); 5: 'Rough Island Interstadial' (after ~ 13.0 ^{14}C ka BP) (McCabe et al., 2007b). Note the
588 close relationship between the main retreat periods of the BIIS and enhanced turbiditic
589 activity in the Whittard channel.

590 **TABLE CAPTION**

591

592 Table 1: Key parameters of cores discussed in this study including core number, geographic
593 position, water depth and oceanographic missions.

594

595 Table 2: Radiocarbon ages of cores MD04-2836, MD03-2688, MD03-2690 and MD03-2695
596 and of the neighbouring core MD95-2002. Radiocarbon ages of this study were performed at
597 the 'Laboratoire de Mesure du Carbone 14' in Saclay ('SacA'). Radiocarbon dates have been
598 corrected for a marine reservoir effect of 400 years and calibrated to calendar years using
599 CALIB Rev 5.0 / Marine04 data set (Hughen et al., 2004; Stuiver and Reimer, 1993; Stuiver
600 et al., 2005) up to 21.78 ¹⁴C ka and Bard et al. (1998) thereafter.

601 **REFERENCES**

- 602
603
604 Auffret, G., Zaragosi, S., Dennielou, B., Cortijo, E., Van Rooij, D., Grousset, F., Pujol, C.,
605 Eynaud, F., Siegert, M., 2002. Terrigenous fluxes at the Celtic margin during the last
606 glacial cycle. *Marine Geology* 188 (1-2), 79-108.
607 Bard, E., 1998. Geochemical and geophysical implications of the radiocarbon calibration.
608 *Geochimica Cosmochimica Acta* 62, 2025-2038.
609 Bard, E., Rostek, F., Turon, J.L., Gendreau, S., 2000. Hydrological impact of Heinrich
610 events in the subtropical Northeast Atlantic. *Science* 289, 1321-1324.
611 Bond, G., Broecker, W., Johnsen, S., McManus, J., Labeyrie, L., Jouzel, J., Bonani, G., 1993.
612 Correlations between climate records from North Atlantic sediments and Greenland ice.
613 *Nature* 365, 143-147.
614 Bond, G., Heinrich, H., Broecker, W., Labeyrie, L., McManus, J., Andrews, J., Huon,
615 Jantschik, R., Clasen, S., Simet, C., Tedesco, K., Klas, M., Bonani, G., Ivy, S., 1992.
616 Evidence for massive discharges of icebergs into the North Atlantic ocean during the
617 last glacial period. *Nature* 360, 245-249.
618 Boulton, G., Hagdorn, M., 2006. Glaciology of the British Isles Ice Sheet during the last
619 glacial cycle: form, flow, streams and lobes. *Quaternary Science Reviews* 25 (23-24),
620 3359-3390.
621 Bouma, A.H., 1962. Sedimentology of some flysch deposits: a graphic approach to facies
622 interpretation. Amsterdam, Elsevier, 168 pp.
623 Bourillet, J.F., Reynaud, J.Y., Baltzer, A., Zaragosi, S., 2003. The "Fleuve Manche": the
624 submarine sedimentary features from the outer shelf to the deep-sea fans. *Journal of*
625 *Quaternary Science* 18 (3-4), 261-282.
626 Bourillet, J.F., Turon, J.L., 2003. Rapport de mission MD133-SEDICAR. 150 pp.
627 Bowen, D.Q., Phillips, F.M., McCabe, A.M., Knutz, P.C., Sykes, G.A., 2002. New data for
628 the Last Glacial Maximum in Great Britain and Ireland. *Quaternary Science Reviews*
629 21 (1-3), 89-101.
630 Bowen, D.Q., Rose, J., McCabe, A.M., Sutherland, D.G., 1986. Correlation of Quaternary
631 glaciations in England, Ireland, Scotland and Wales. *Quaternary Science Reviews* 5,
632 299-340.
633 Buoncristiani, J.F., Campy, M., 2004. Expansion and retreat of the Jura ice sheet (France)
634 during the last glacial maximum. *Sedimentary Geology* 165, 253-264.
635 Chapman, M.R., Shackleton, N.J., Duplessy, J.C., 2000. Sea surface temperature variability
636 during the last glacial-interglacial cycle: Assessing the magnitude and pattern of
637 climate change in the North Atlantic. *Palaeogeography, Palaeoclimatology,*
638 *Palaeoecology* 157 (1-2), 1-25.
639 Chappell, J., 2002. Sea level changes forced ice breakouts in the Last Glacial cycle: new
640 results from coral terraces. *Quaternary Science Reviews* 21 (10), 1229-1240.
641 Clark, P.U., McCabe, A.M., Mix, A.C., Weaver, A.J., 2004. Rapid sea level rise at 19,000
642 years ago and its global implications. *Science* 304, 1141-1144, doi:
643 10.1126/science.1094449.
644 Clarke, G.K.C., Marshall, S.J., Hillaire-Marcel, C., Bilodeau, G., Veiga-Pires, C., 1999. A
645 glaciological perspective on Heinrich events. In *Mechanisms of Global Climate*
646 *Change at Millennial Time Scales*, P. U. Clark, R.S. Webb, and L. D. Keigwin (Eds.),
647 AGU Geophys. Monograph 112, Washington D.C., pp. 243-262.

- 648 Dahlgren, K.I.T., Vorren, T.O., 2003. Sedimentary environment and glacial history during the
649 last 40 ka of the Voring continental margin, mid-Norway. *Marine Geology* 193, 93-
650 127.
- 651 Dansgaard, W., Johnsen, S.J., Clausen, H.B., Dahl-Jensen, D., Gundestrup, N.S., Hammer,
652 C.U., Hvidberg, C.S., Steffensen, J.P., Sveinbjörnsdottir, A.E., Jouzel, J., Bond, G.,
653 1993. Evidence for general instability of past climate from 250-kyr ice-core record.
654 *Nature* 364, 218-220.
- 655 Dowdeswell, J.A., O’Cofaigh, C., Taylor, J., Kenyon, N.H., Mienert, J., Wilken, M., 2002.
656 On the architecture of high-latitude continental margins: the influence of ice-sheet and
657 sea-ice processes in the Polar North Atlantic. *in*: Dowdeswell, J.A. & O’Cofaigh C.
658 (eds) 2002. *Glacier-Influenced Sedimentation on High-Latitude Continental Margins*.
659 Geological Society, London, Special Publications. 203, 33-54.
- 660 Droz, L., Auffret, G.A., Savoye, B., Bourillet, J.F., 1999. L'éventail profond de la marge
661 Celtique : stratigraphie et évolution sédimentaire. *C.R. Acad. Sci. Paris* 328, 173-180.
- 662 Elliot, M., Labeyrie, L., Dokken, T., Manthe, S., 2001. Coherent patterns of ice-rafted debris
663 deposits in the Nordic regions during the last glacial (10-60 ka). *Earth and Planetary*
664 *Science Letters* 194 (1-2), 151-163.
- 665 Elverhoi, A., Hooke, R.L., Solheim, A., 1998. Late Cenozoic erosion and sediment yield from
666 the Svalbard-Barents Sea region: implications for the understanding of glacierized
667 basins. *Quaternary Sciences Reviews* 17, 209-241.
- 668 Evans, D.J.A., O’Cofaigh, C., 2003. Depositional evidence for marginal oscillations of the
669 Irish Sea ice stream in southeast Ireland during the last glaciation. *Boreas* 32, 76-101.
- 670 Everest, J.D., Bradwell, T., Fogwill, C.J., Kubik, P.W., 2006. Cosmogenic 10BE age
671 constraints for the Wester Ross Readvance moraine: Insights into British Ice-Sheet
672 behaviour. *Geografiska Annaler, Series A: Physical Geography* 88 (1), 9-17.
- 673 Eyles, N., McCabe, A., 1989. The Late Devensian (<22,000 BP) Irish Sea Basin: The
674 sedimentary record of a collapsed ice sheet margin. *Quaternary Science Reviews* 8 (4),
675 307-351.
- 676 Eynaud, F., 1999. Kystes de dinoflagellés et évolution paléoclimatique et paléohydrologique
677 de l'Atlantique Nord au cours du dernier cycle climatique du Quaternaire. Thèse de
678 doctorat, Université Bordeaux 1, 291.
- 679 Eynaud, F., Zaragosi, S., Scourse, J.D., Mojtahid, M., Bourillet, J.F., Hall, I.R., Penaud, A.,
680 Locascio, M., Reijonen, A., 2007. Deglacial laminated facies on the NW European
681 continental margin: the hydrographic significance of British Ice sheet deglaciation and
682 Fleuve Manche paleoriver discharges. *Geochemistry, Geophysics, Geosystems* 8 (1),
683 doi:10.1029/2006GC001496.
- 684 Fairbanks, R.G., 1989. A 17,000-year glacioeustatic sea level record: Influence of glacial
685 melting on the Younger Dryas event and deep-ocean circulation. *Nature* 342, 637-642.
- 686 Forsström, P.L., Greve, R., 2004. Simulation of the Eurasian ice sheet dynamics during the
687 last glaciation. *Global and Planetary Change* 42, 59-81.
- 688 Gilbert, R., Nielsen, N., Moller, H., Desloges, J.R., Rasch, M., 2002. Glacimarine
689 sedimentation in Kangerdluk (Disko Fjord), West Greenland, in response to a surging
690 glacier. *Marine Geology* 191 (1-2), 1-18.
- 691 Grousset, F.E., Pujol, C., Labeyrie, L., Auffret, G., Boelaert, A., 2000. Were the North
692 Atlantic Heinrich events triggered by the behavior of the European ice sheets?
693 *Geology* 28 (2), 123-126.
- 694 Hesse, R., Rashid, H., Khodabakhsh, S., 2004. Fine-grained sediment lofting from meltwater-
695 generated turbidity currents during Heinrich events. *Geology* 32 (5), 449-452.

696 Hiemstra, J.F., Evans, D.J.A., Scourse, J.D., McCarroll, D., Furze, M.F.A., Rhodes, E., 2006.
697 New evidence for a grounded Irish Sea glaciation of the Isles of Scilly, UK.
698 *Quaternary Science Reviews* 25, 299-309.

699 Hinderer, M., 2001. Late Quaternary denudation of the Alps, valley and lake fillings and
700 modern river loads. *Geodinamica Acta* 14, 231-263.

701 Hughen, K.A. et al., 2004. Marine04 Marine Radiocarbon Age Calibration, 0–26 Cal Kyr BP.
702 *Radiocarbon* 46, 1059-1086.

703 Ivy-Ochs, S., Kerschner, H., Kubik, P.W., Schlüchter, C., 2006. Glacier response in the
704 European Alps to Heinrich Event 1 cooling: the Gschnitz stadial. *Journal of*
705 *Quaternary Science* 21 (2), 115-130.

706 Ivy-Ochs, S., Schäfer, J., Kubik, P.W., Synal, H.-A., Schlüchter, C., 2004. Timing of
707 deglaciation on the northern Alpine foreland (Switzerland). *Eclogae Geologicae*
708 *Helveticae* 97 (1), 47-55.

709 Knies, J., Vogt, C., Matthiessen, J., Nam, S.I., Ottesen, D., Rise, L., Bargel, T., Eilertsen,
710 R.S., 2007. Re-advance of the Fennoscandian Ice Sheet during Heinrich Event 1.
711 *Marine Geology* 240 (1-4), 1-18.

712 Knutz, P.C., Hall, M.A., Zahn, R., Rasmussen, T.L., Kuijpers, A., Moros, M., Shackleton,
713 N.J., 2002a. Multidecadal ocean variability and NW European ice sheet surges during
714 the last deglaciation. *Geochemistry, Geophysics, Geosystems* 3 (12), 1077,
715 doi:10.1029/2002GC000351.

716 Knutz, P.C., Jones, E.J.W., Austin, W.E.N., van Weering, T.C.E., 2002b. Glacimarine slope
717 sedimentation, contourite drifts and bottom current pathways on the Barra Fan, UK
718 North Atlantic margin. *Marine Geology* 188 (1-2), 129-146.

719 Knutz, P.C., Zahn, R., Hall, I.R., 2007. Centennial-scale variability of the British Ice Sheet:
720 Implications for climate forcing and atlantic meridional overturning circulation during
721 the last deglaciation. *Paleoceanography* 22 (PA1207, doi:10.1029/2006PA001298).

722 Kucera, M., Rosell-Mele, A., Schneider, R., Waelbroeck, C., Weinelt, M., 2005. Multiproxy
723 approach for the reconstruction of the glacial ocean surface (MARGO). *Quaternary*
724 *Science Reviews* 24 (7-9), 813-819.

725 Lambeck, K., Yokoyama, Y., Purcell, T., 2002. Into and out of the Last Glacial Maximum:
726 sea-level change during Oxygen Isotope Stages 3 and 2. *Quaternary Science Reviews*
727 21 (1-3), 343-360.

728 Larssonneur, C., Auffret, J.P., Smith, A.J., 1982. Carte des paléo-vallées et des bancs de la
729 Manche orientale (1/50 000). BRGM, Brest.

730 Le Suavé, R., 2000. Synthèse bathymétrique et imagerie acoustique. zone économique
731 exclusive (ZEE). Atlantique nord-Est, Brest, Editions IFREMER.

732 Lekens, W.A.H., Sejrup, H.P., Haflidason, H., Petersen, G.O., Hjelstuen, B., Knorr, G., 2005.
733 Laminated sediments preceding Heinrich event 1 in the Northern North Sea and
734 Southern Norwegian Sea: Origin, processes and regional linkage. *Marine Geology* 216
735 (1-2), 27-50.

736 Lericolais, G., 1997. Evolution du Fleuve Manche depuis l'Oligocène: stratigraphie et
737 géomorphologie d'une plate-forme continentale en régime périglaciaire. Thèse de
738 doctorat, Université Bordeaux 1, 265 pp.

739 Mansor, S., 2004. Faciès sismique et architecture du système turbiditique armoricain. Rapport
740 de Diplôme d'Etudes Approfondi. Université de Bretagne Occidentale. 51 pp.
741 (available online via the ASF website: <http://www.sedimentologie.com>).

742 Marks, L., 2002. Last Glacial Maximum in Poland. *Quaternary Science Reviews* 21 (1-3),
743 103-110.

744 McCabe, A.M., Clark, P.U., 1998. Ice-sheet variability around the North Atlantic Ocean
745 during the last deglaciation. *Nature* 392, 373-376.

- 746 McCabe, A.M., Clark, P.U., Clark, J., 2005. AMS 14C dating of deglacial events in the Irish
747 Sea Basin and other sectors of the British-Irish ice sheet. *Quaternary Science Reviews*
748 24 (14-15), 1673-1690.
- 749 McCabe, A.M., Clark, P.U., Clark, J., 2007a. Radiocarbon constraints on the history of the
750 western Irish ice sheet prior to the Last Glacial Maximum. *Geology* 35 (2), 147-150.
- 751 McCabe, A.M., Clark, P.U., Clark, J., Dunlop, P., 2007b. Radiocarbon constraints on
752 readvances of the British-Irish Ice Sheet in the northern Irish Sea Basin during the last
753 deglaciation. *Quaternary Science Reviews* 26 (9-10), 1204-1211.
- 754 Ménot, G., Bard, E., Rostek, F., Weijers, J.W.H., E.C., H., Schouten, S., Sinninghe Damsté,
755 J.S., 2006. Early reactivation of European Rivers during the last deglaciation. *Science*
756 313, 1623-1625.
- 757 Migeon, S., Weber, O., Faugères, J.-C., Saint-Paul, J., 1999. SCOPIX: A new X-ray imaging
758 system for core analysis. *Geo-Marine Letters* 18, 251-255.
- 759 Mix, A.C., Bard, E., Schneider, R., 2001. Environmental processes of the ice age: land,
760 oceans, glaciers (EPILOG). *Quaternary Science Reviews* 20, 627-657.
- 761 Mojtahid, M., Eynaud, F., Zaragosi, S., Scourse, J., Bourillet, J.F., Garlan, T., 2005.
762 Palaeoclimatology and palaeohydrography of the glacial stages on Celtic and
763 Armorican margins over the last 360 000 yrs. *Marine Geology* 224 (1-4), 57-82.
- 764 Naughton, F., Sanchez Goni, M.F., Desprat, S., Turon, J.L., Duprat, J., Malaize, B., Joli, C.,
765 Cortijo, E., Drago, T., Freitas, M.C., 2007. Present-day and past (last 25 000 years)
766 marine pollen signal off western Iberia. *Marine Micropaleontology* 62 (2), 91-114.
- 767 Naughton, F., Sanchez Goni, M.F., Duprat, J., Cortijo, E., Malaize, B., Joly, C., Bard, E.,
768 Rostek, F., Turon, J.L., Wet to dry trend in north western Iberia within Heinrich
769 events. *Earth and Planetary Science Letters*, submitted.
- 770 Nygard, A., Sejrup, H.P., Hafliðason, H., Cecchi, M., Ottesen, D., 2004. Deglaciation history
771 of the southwestern Fennoscandian Ice Sheet between 15 and 13 ¹⁴C ka BP. *Boreas*
772 33, 1-17.
- 773 O'Cofaigh, C., Evans, D.J.A., 2007. Radiocarbon constraints on the age of the maximum
774 advance of the British-Irish Ice Sheet in the Celtic Sea. *Quaternary Science Reviews*
775 26 (9-10), 1197-1203.
- 776 Peck, V.L., Hall, I.R., Zahn, R., Elderfield, H., Grousset, F., Hemming, S.R., Scourse, J.D.,
777 2006. High resolution evidence for linkages between NW European ice sheet
778 instability and Atlantic Meridional Overturning Circulation. *Earth and Planetary*
779 *Science Letters* 243 (3-4), 476-488.
- 780 Peck, V.L., Hall, I.R., Zahn, R., Grousset, F., Hemming, S.R., Scourse, J.D., 2007. The
781 relationship of Heinrich events and their European precursors over the past 60 ka BP:
782 a multi-proxy ice-rafted debris provenance study in the North East Atlantic.
783 *Quaternary Science Reviews* 26, 862-875.
- 784 Posamentier, H.W., Vail, P.R., 1988. Eustatic controls on clastic deposition II — Sequence
785 and systems tract models. In: Wilgus, Ch.K. et al. (Eds.), *Sea-level Changes: an*
786 *Integrated Approach*. Soc. Econ. Paleontol. Mineral. Spec. Publ. 42, 125-154.
- 787 Rashid, H., Hesse, R., Piper, D.J.W., 2003. Origin of unusually thick Heinrich layers in ice-
788 proximal regions of the northwest Labrador Sea. *Earth and Planetary Science Letters*
789 208 (3-4), 319-336.
- 790 Reynaud, J.Y., Tessier, B., Proust, J.N., Dalrymple, R., Marsset, T., DeBatist, M., Bourillet,
791 J.F., Lericolais, G., 1999. Eustatic and hydrodynamic controls on the architecture of a
792 deep shelf sand bank (Celtic Sea). *Sedimentology* 46 (4), 703-721.
- 793 Rinterknecht, V.R., Clark, P.U., Raisbeck, G.M., Yiou, F., Bitinas, A., Brook, E.J., Marks, L.,
794 Zelcs, V., Lunkka, J.P., Pavlovskaya, I.E., Piotrowski, J.A., Raukas, A., 2006. The

795 Last Deglaciation of the Southeastern Sector of the Scandinavian Ice Sheet. *Science*
796 311 (5766), 1449-1452.

797 Scourse, J.D., 1991. Late Pleistocene stratigraphy and palaeobotany of the Isles of Scilly.
798 *Philosophical Transactions of the Royal Society of London* B334, 405-448.

799 Scourse, J.D., Austin, W.E.N., Bateman, R.M., Catt, J.A., Evans, C.D.R., Robinson, J.E.,
800 Young, J.R., 1990. Sedimentology and micropaleontology of glacial marine sediments
801 from the Central and Southwestern Celtic Sea. *Special Publication of the Geological*
802 *Society of London* 53, 329-347.

803 Scourse, J.D., Furze, M.F.A., 2001. A critical review of the glaciomarine model for Irish sea
804 deglaciation: evidence from southern Britain, the Celtic shelf and adjacent continental
805 slope. *Journal of Quaternary Science* 16 (5), 419-434.

806 Siddall, M., Rohling, E.J., Almogi-Labin, A., Hemleben, C., Meischner, D., Scheizmer, I.,
807 Smeed, D.A., 2003. Sea-level fluctuations during the last glacial cycle. *Nature* 423,
808 853-858.

809 Skinner, L.C., McCave, I.N., 2003. Analysis and modelling of gravity- and piston coring
810 based on soil mechanics. *Marine Geology* 199 (1-2), 181-204.

811 Stow, D.A.V., Piper, D.J.W., 1984. Deep-water fine-grained sediments: facies model. Fine-
812 grained sediments: deep-water processes and facies. *Geological Society, Special*
813 *Publication* 15, 611-645.

814 Stuiver, M., Reimer, P.J., 1993. Extended ¹⁴C data base and revised CALIB radiocarbon
815 calibration program. *Radiocarbon* 35, 215-230.

816 Stuiver, M., Reimer, P.J., Reimer, R.W., 2005. CALIB 5.0. [WWW program and
817 documentation].

818 Turon, J.L., Bourillet, J.F., 2004. Rapport de mission MD141-ALIENOR. 45 pp.

819 Uehara, K., Scourse, J.D., Horsburgh, K.J., Lambeck, K., Purcell, A.P., 2006. Tidal evolution
820 of the northwest European shelf seas from the Last Glacial Maximum to the present.
821 *Journal of Geophysical Research* 111, C09025, doi:10.1029/2006JC003531.

822 Watts, W.A., 1980. regional variation in the response of vegetation to Lateglacial climatic
823 events in Europe. Lowe, J.J., Gray, J.M., Robinson, J.E. (Eds), *Studies in the*
824 *Lateglacial of North West Europe*. Pergamon Press, Oxford, pp.1-22.

825 Weaver, P.P.E., Benetti, S., 2006. The North Atlantic deep-sea floor - glacial versus
826 interglacial controls and comparisons between the eastern and western North Atlantic.
827 *Geophysical Research Abstracts*, vol. 8, 10678.

828 Weaver, P.P.E., Wynn, R.B., Kenyon, N.H., Evans, J., 2000. Continental margin
829 sedimentation, with special reference to the north-east Atlantic margin. *Sedimentology*
830 47 (1), 239-256.

831 Wilson, L.J., Austin, W.E.N., Jansen, E., 2002. The last British Ice Sheet: growth, maximum
832 extent and deglaciation. *Polar Research* 21 (2), 243-250.

833 Yokoyama, Y., Lambeck, K., De Deckker, P., Johnston, P., Fifield, L.K., 2000. Timing of the
834 Last Glacial Maximum from observed sea-level minima. *Nature* 406, 713-716.

835 Zaragosi, Le, S., Bourillet, Auffret, Faugères, Pujol, Garlan, 2001a. The deep-sea Armorican
836 depositional system (Bay of Biscay), a multiple source, ramp model. *Geo-Marine*
837 *Letters* 20 (4), 219-232.

838 Zaragosi, S., Auffret, G.A., Faugeres, J.C., Garlan, T., Pujol, C., Cortijo, E., 2000.
839 Physiography and recent sediment distribution of the Celtic Deep-Sea Fan, Bay of
840 Biscay. *Marine Geology* 169 (1-2), 207-237.

841 Zaragosi, S., Bourillet, J.F., Eynaud, F., Toucanne, S., Denhard, B., Van Toer, A., Lanfumey,
842 V., 2006. The impact of the last European deglaciation on the deep-sea turbidite
843 systems of the Celtic-Armorican margin (Bay of Biscay). *Geo-Marine Letters* V26 (6),
844 317-329.

845 Zaragosi, S., Eynaud, F., Pujol, C., Auffret, G.A., Turon, J.L., Garlan, T., 2001b. Initiation of
846 the European deglaciation as recorded in the northwestern Bay of Biscay slope
847 environments (Meriadzek Terrace and Trevelyan Escarpment): a multi-proxy
848 approach. *Earth and Planetary Science Letters* 188 (3-4), 493-507.
849
850

Table1
[Click here to download Table: table_1.xls](#)

Core number	Latitude	Longitude	Depth (m)	Cruise	Year	institute
MD952002	47° 27.12' N	08° 32.03' W	2.174	MD 105 IMAGE 1	1995	IFREMER
MD032688	46° 48.03' N	07° 02.93' W	4.385	MD 133 SEDICAR	2003	IFREMER
MD032690	47° 01.25' N	07° 44.99' W	4.340	MD 133 SEDICAR	2003	IFREMER
MD032695	47° 43,14' N	06° 12,68' W	4.375	MD 133 SEDICAR	2003	IFREMER
MD042836	47° 16.57' N	10° 07.69' W	4.362	MD 141 ALIENOR	2004	IFREMER
MD042837	47° 31.99' N	09° 44.01' W	4.176	MD 141 ALIENOR	2004	IFREMER

Table2

[Click here to download Table: table_2.xls](#)

Core number	Depth (cm)	Material	Laboratory Number	Corrected ¹⁴ C age (yr BP)	Calendar age (cal yr BP)	Data origin
MD95-2002	0	<i>G. Bulloides</i>	LSCCE-99360	1660 +/- 70	1624	Zaragosi et al., 2001
MD95-2002	140	<i>G. Bulloides</i>	LSCCE-99361	9080 +/- 90	10329	Zaragosi et al., 2001
MD95-2002	240	<i>N. pachyderma</i> s.	LSCCE-99362	10790 +/- 100	12809	Zaragosi et al., 2001
MD95-2002	420	<i>N. pachyderma</i> s.	LSCCE-99363	13330 +/- 130	15798	Zaragosi et al., 2001
MD95-2002	454	<i>N. pachyderma</i> s.	LSCCE-99364	13800 +/- 110	16426	Zaragosi et al., 2001
MD95-2002	463	<i>N. pachyderma</i> s.	LSCCE-99365	14020 +/- 120	16709	Zaragosi et al., 2001
MD95-2002	510	<i>N. pachyderma</i> s.	LSCCE-99366	14170 +/- 130	16897	Zaragosi et al., 2001
MD95-2002	550	<i>N. pachyderma</i> s.	SacA-003242	14430 +/- 70	17327	Zaragosi et al., 2006
MD95-2002	580	<i>N. pachyderma</i> s.	Beta-141702	14410 +/- 200	17332	Zaragosi et al., 2001
MD95-2002	869	<i>N. pachyderma</i> s.	SacA-003243	14900 +/- 70	18241	Zaragosi et al., 2006
MD95-2002	875	<i>N. pachyderma</i> s.	SacA-003244	14880 +/- 160	18224	Zaragosi et al., 2006
MD95-2002	1320	<i>G. Bulloides</i>	SacA-003245	18450 +/- 90	22062	Zaragosi et al., 2006
MD95-2002	1340	<i>G. Bulloides</i>	SacA-003246	19030 +/- 100	22514	Zaragosi et al., 2006
MD95-2002	1390	<i>G. Bulloides</i>	SacA-003247	20220 +/- 80	24690	Zaragosi et al., 2006
MD95-2002	1424	<i>N. pachyderma</i> s.	Beta-123696	19840 +/- 60	23777	Grousset et al., 2000
MD95-2002	1453	<i>N. pachyderma</i> s.	Beta-123698	20030 +/- 80	23984	Grousset et al., 2000
MD95-2002	1464	<i>N. pachyderma</i> s.	Beta-123699	20200 +/- 80	24174	Grousset et al., 2000
MD95-2002	1534	<i>N. pachyderma</i> s.	Beta-123697	21850 +/- 70	25734	Grousset et al., 2000
MD95-2002	1610	<i>N. pachyderma</i> s.	Beta-99367	24010 +/- 250	28222	Auffret et al., 2002
MD95-2002	1664	<i>N. pachyderma</i> s.	Beta-99368	25420 +/- 230	29830	Auffret et al., 2002
MD04-2836	100.5			9275	10700	correlation MD95-2002
MD04-2836	150.5	<i>N. pachyderma</i> s.	SacA-003248	10730+/-50	12788	Zaragosi et al., 2006
MD04-2836	411.5			11900	13938	correlation MD95-2002
MD04-2836	1354.5	<i>N. pachyderma</i> s.	SacA-003249	12840+/-120	15159	Zaragosi et al., 2006
MD04-2836	1656.5	<i>N. pachyderma</i> s.	SacA-003253	13480+/-60	16017	Zaragosi et al., 2006
MD04-2836	1761.5	<i>N. pachyderma</i> s.	SacA-003254	14210+/-70	16956	Zaragosi et al., 2006
MD04-2836	2131.5	<i>N. pachyderma</i> s.	SacA-005971	14650+/-50	17727	this paper
MD04-2836	2534.5			15091	18396	correlation MD95-2002
MD04-2836	3525.5	<i>N. pachyderma</i> s.	SacA-003256	17090+/-80	20209	Zaragosi et al., 2006
MD03-2688	157	<i>G. bulloides</i>	SacA-004927	8495 +/- 35	9541	this paper
MD03-2688	480	<i>N. pachyderma</i> s.	SacA-004928	12580 +/- 90	14751	this paper
MD03-2688	1084	<i>N. pachyderma</i> s.	SacA-004929	14200 +/- 70	16941	this paper
MD03-2688	1704	<i>N. pachyderma</i> s.	SacA-004930	14650 +/- 110	17699	this paper
MD03-2688	1955			15091	18396	correlation MD95-2002
MD03-2688	2422	<i>G. bulloides</i>	SacA-004931	16930 +/- 80	20057	this paper
MD03-2688	2695			20220	23722	correlation MD95-2002
MD03-2688	2910	<i>N. pachyderma</i> s.	SacA-004932	21570 +/- 110	25410	this paper
MD03-2688	3136	<i>N. pachyderma</i> s.	SacA-004933	24890 +/- 140	29227	this paper
MD03-2688	3520	<i>G. bulloides</i>	SacA-004793	29160 +/- 180	34038	this paper
MD03-2690	151	<i>G. Bulloides</i>	SacA-001894	8730 +/- 60	9900	Zaragosi et al., 2006
MD03-2690	245	<i>G. Bulloides</i>	SacA-003233	9450 +/- 60	10774	Zaragosi et al., 2006
MD03-2690	425			11900	13938	correlation MD95-2002
MD03-2690	626	<i>G. Bulloides</i>	SacA-003234	12620 +/- 60	14863	Zaragosi et al., 2006
MD03-2690	692	<i>N. pachyderma</i> s.	SacA-003235	12770 +/- 70	15074	Zaragosi et al., 2006
MD03-2690	1094	<i>N. pachyderma</i> s.	SacA-003236	13840 +/- 70	16483	Zaragosi et al., 2006
MD03-2690	1213	<i>N. pachyderma</i> s.	SacA-003237	14030 +/- 70	16715	Zaragosi et al., 2006
MD03-2690	1885	<i>N. pachyderma</i> s.	SacA-003238	14650 +/- 70	17717	Zaragosi et al., 2006
MD03-2690	2233	<i>N. pachyderma</i> s.	SacA-003239	14960 +/- 70	18287	Zaragosi et al., 2006
MD03-2690	2276	<i>N. pachyderma</i> s.	Poz. Rad. Lab.	15080 +/- 70	18392	Zaragosi et al., 2006
MD03-2690	2923	<i>G. Bulloides</i>	SacA-005972	16990 +/- 110	20115	this paper
MD03-2690	3156	<i>G. Bulloides</i>	SacA-003240	18850 +/- 100	22378	Zaragosi et al., 2006
MD03-2690	3376	<i>N. pachyderma</i> s.	SacA-003241	20560 +/- 70	24600	Zaragosi et al., 2006
MD03-2690	3576	<i>N. pachyderma</i> s.	Poz. Rad. Lab.	21880 +/- 120	25769	Zaragosi et al., 2006
MD03-2695	242			13463	15970	correlation MD95-2002
MD03-2695	878	<i>N. pachyderma</i> s.	SacA-005609	14640+/-60	17703	this paper
MD03-2695	1187.5	<i>N. pachyderma</i> s.	SacA-005610	14830+/- 60	18030	this paper
MD03-2695	1347	<i>N. pachyderma</i> s.	SacA-005611	14990+/- 60	18305	this paper
MD03-2695	1420			15091	18396	correlation MD95-2002
MD03-2695	1991	<i>N. pachyderma</i> s.	SacA-005612	17130+/- 70	20248	this paper
MD03-2695	2255	<i>N. pachyderma</i> s.	SacA-005613	20300+/- 100	24284	this paper
MD03-2695	2393			22,028.2	26032	correlation MD95-2002
MD03-2695	2444	<i>N. pachyderma</i> s.	SacA-005614	25600+/- 150	30034.4	this paper
MD03-2695	2600			27,400	32068	Elliot et al., 2001 (HE3)
MD03-2695	2758	<i>N. pachyderma</i> s.	SacA-005616	28710+/- 210	33536.2	this paper

Figure1
[Click here to download high resolution image](#)

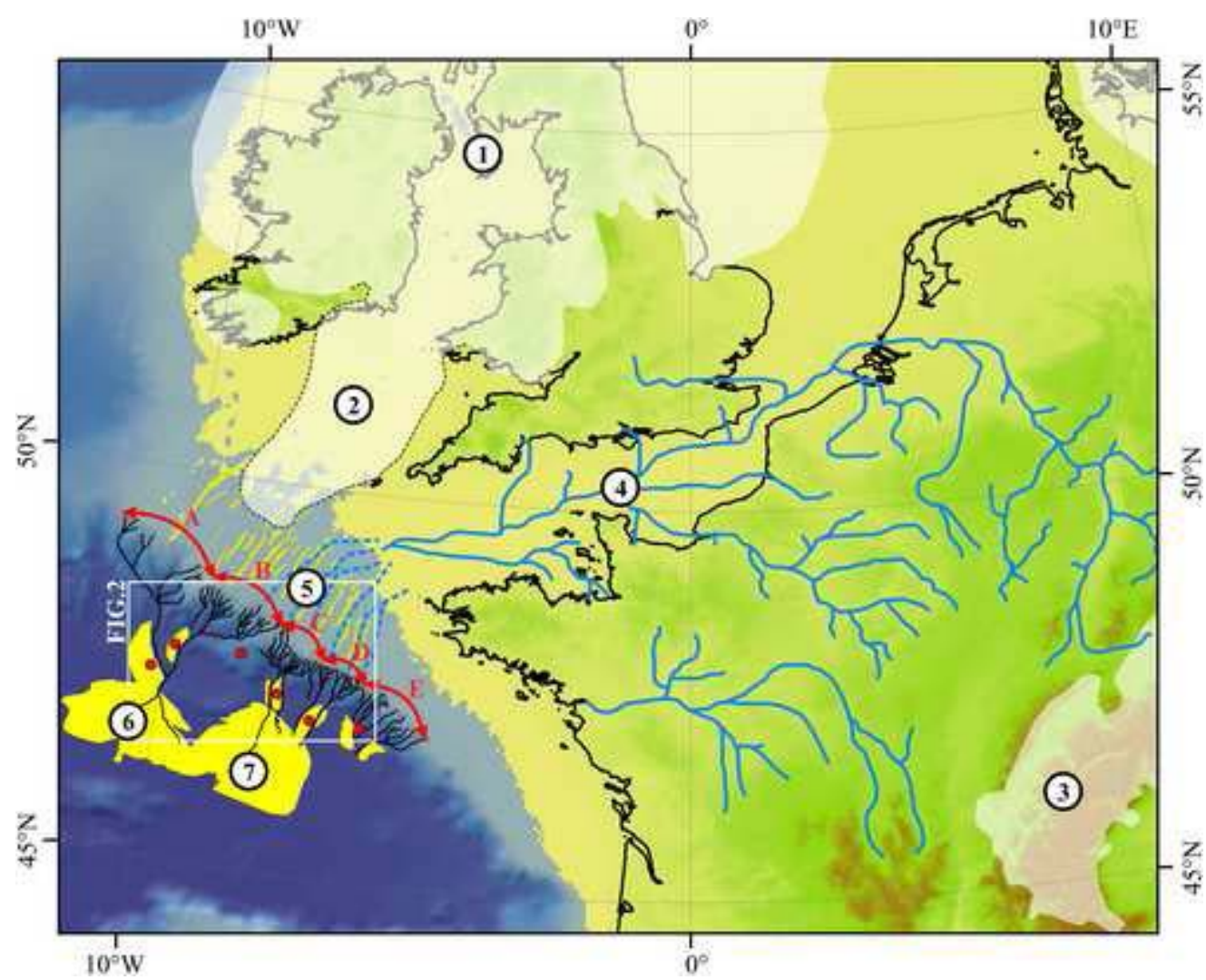


Figure2
[Click here to download high resolution image](#)

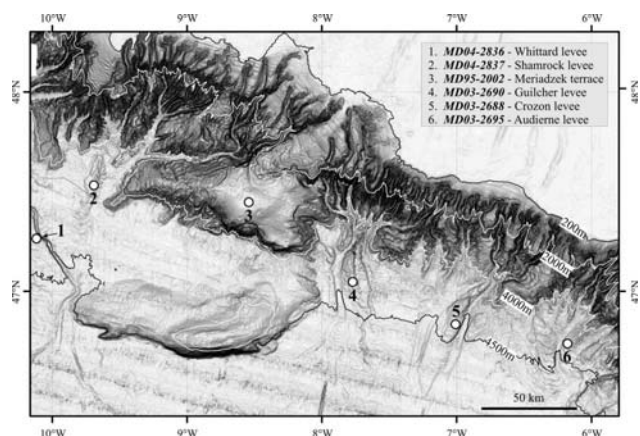


Figure3
[Click here to download high resolution image](#)

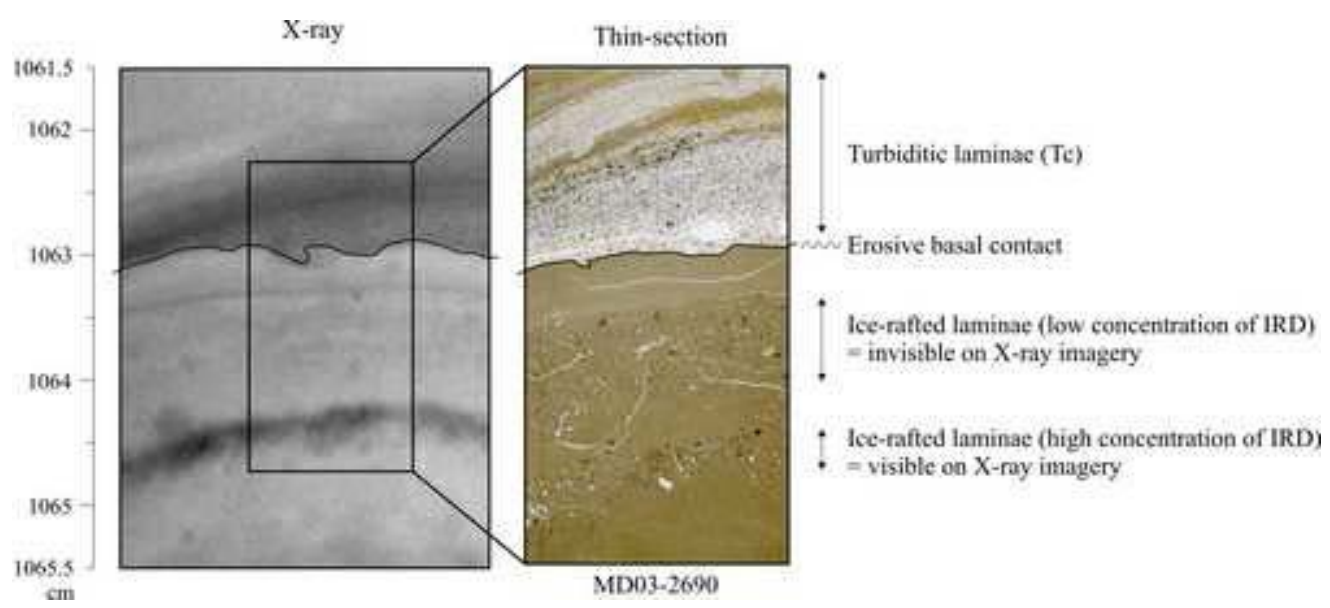


Figure4
[Click here to download high resolution image](#)

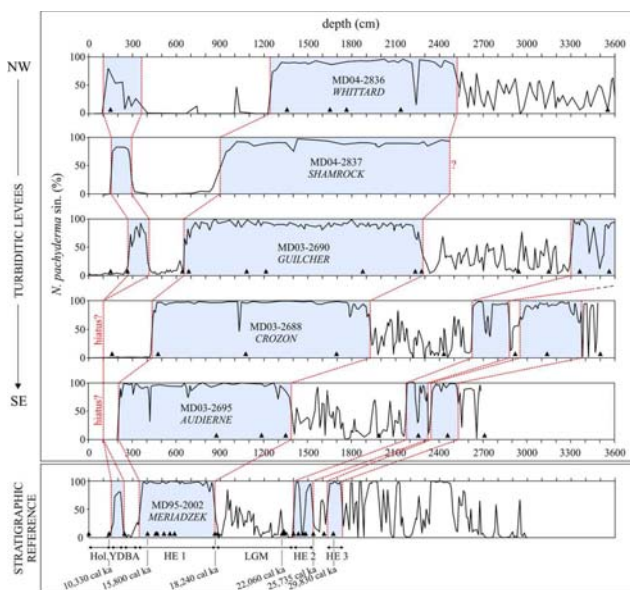


Figure5
[Click here to download high resolution image](#)

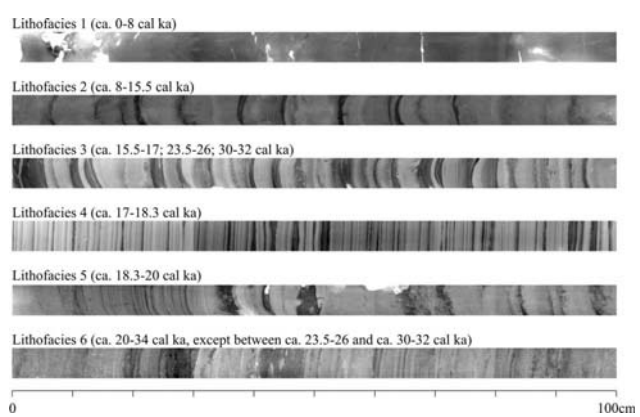


Figure6
[Click here to download high resolution image](#)

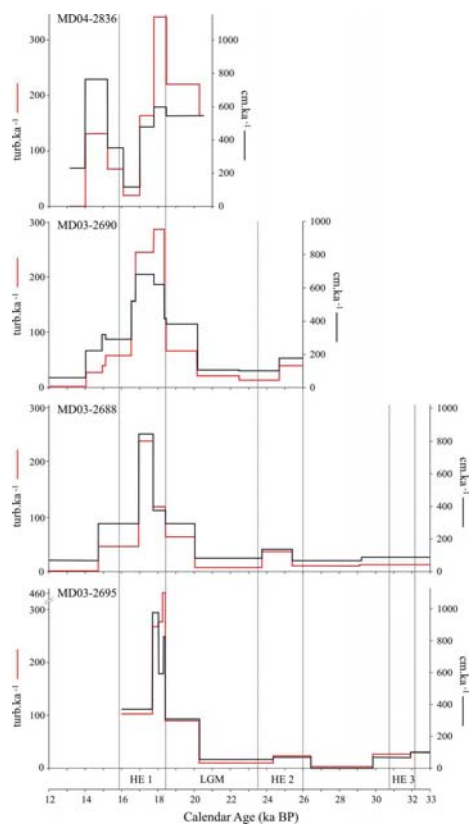


Figure7
[Click here to download high resolution image](#)

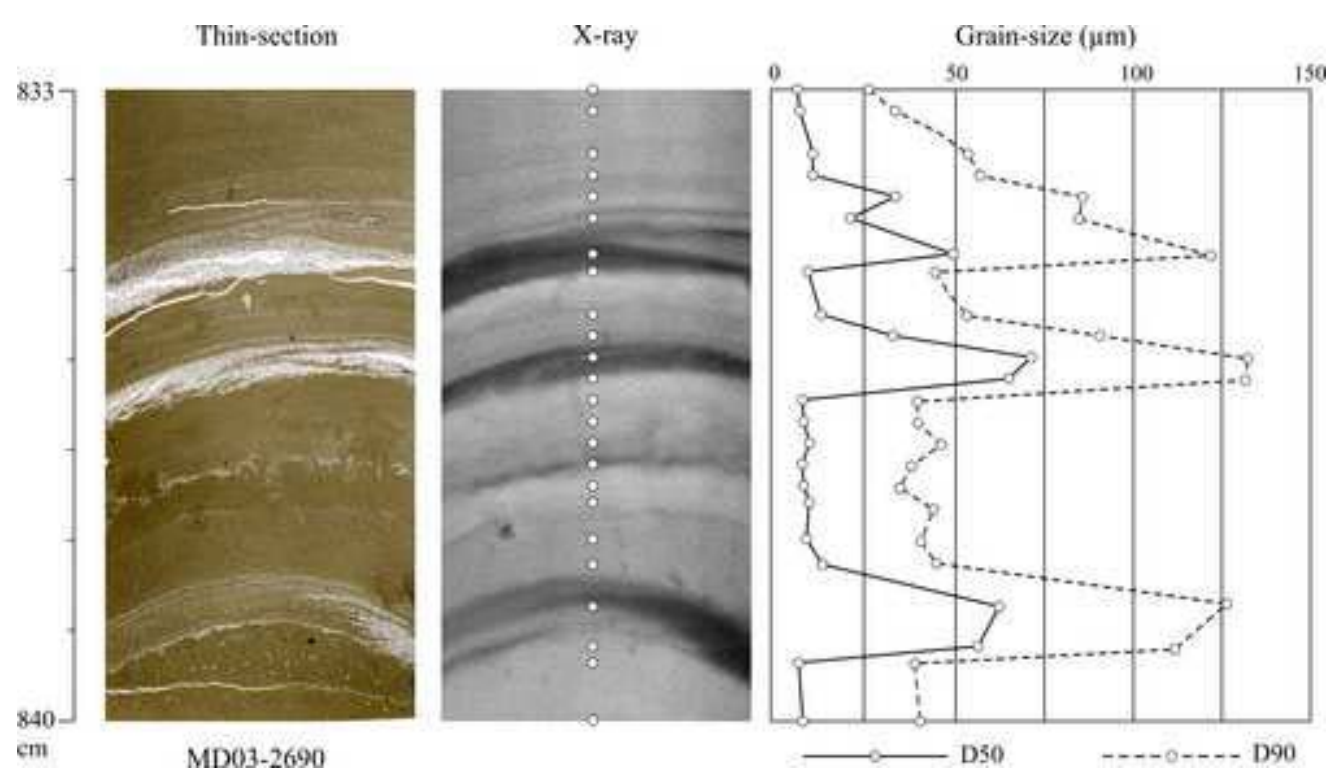


Figure8
[Click here to download high resolution image](#)

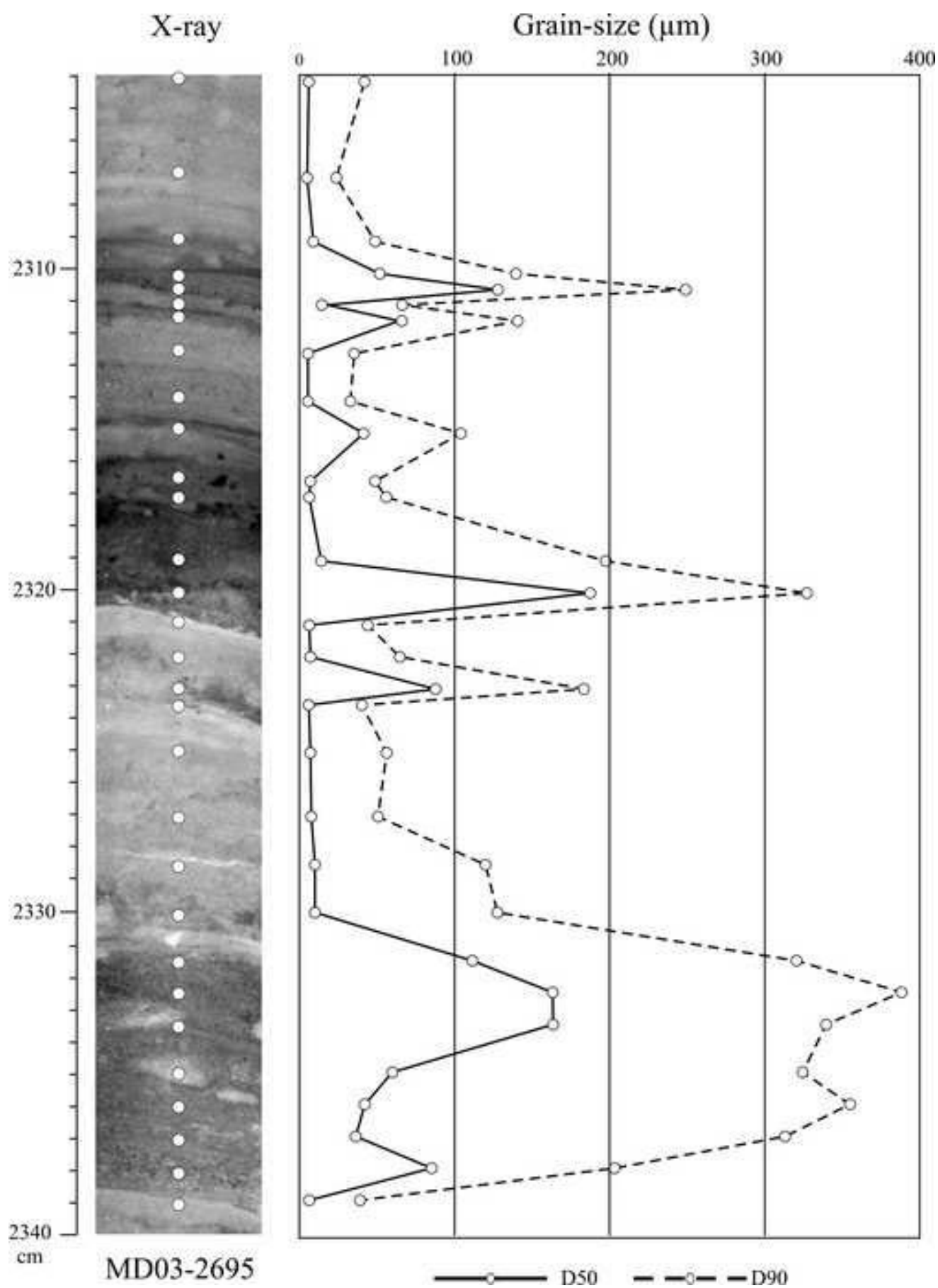


Figure9
[Click here to download high resolution image](#)

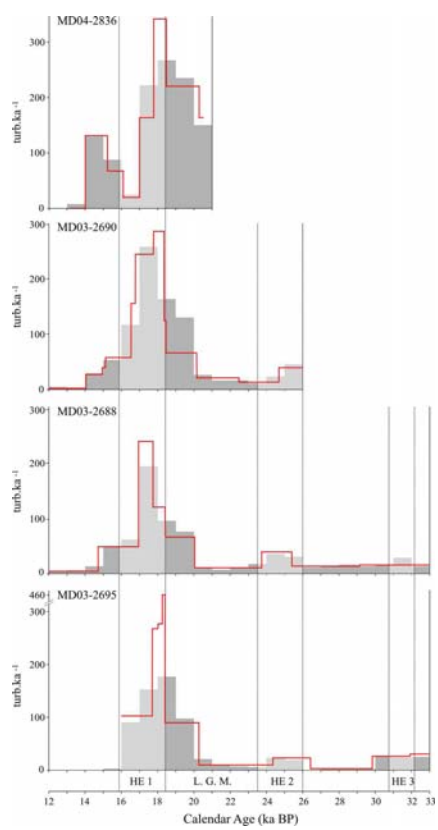


Figure10
[Click here to download high resolution image](#)

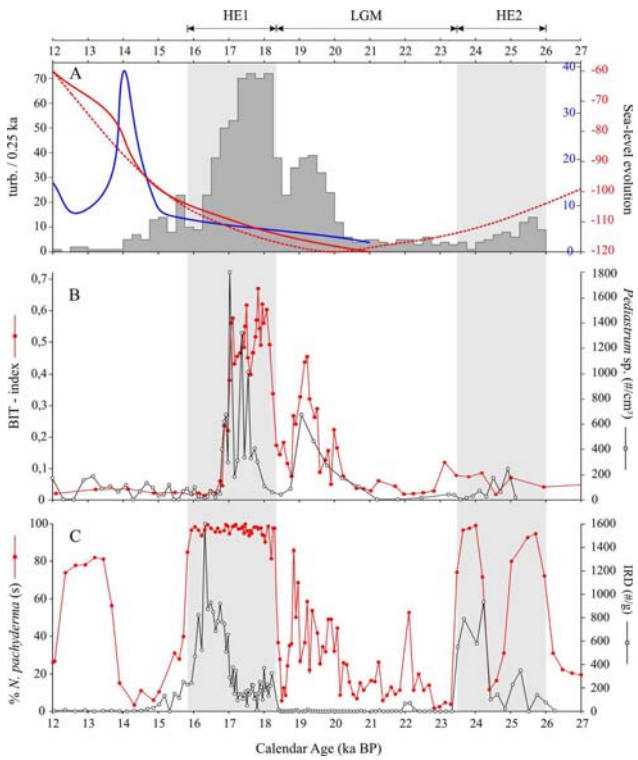


Figure11
[Click here to download high resolution image](#)

